GKU Journal of Multidisciplinary Research (GKUJMR)

Computational Investigation of Hybrid Ferrofluid Flow in Porous L-Shaped Cavity with Circular Cylinder

[1] M.A.R. Pramanik, [2] Md. Sifuzzaman, [3] Rabeya Sarker

[1,2] Department of Computer Science & Engineering, Dhaka International University (DIU), Dhaka-1212, Bangladesh.
[3] Department of Business Administration, Dhaka International University (DIU), Dhaka-1212, Bangladesh
Email: [1] pramanikanis@gmail.com, [2] zaman001217@gmail.com, [3] rabeya835@gmail.com

Accepted: 26.11.2025 Published: 26.12.2025 DOI: 10.5281/zenodo.18409752

Abstract – Hybrid nanofluids (HNFs) have become advanced working fluids because they have better thermo-physical properties and can enhance heat transfer (HT) in complicated thermal systems. This study examines the improvement of heat transmission in an L-shaped porous enclosure featuring a centrally located circular cylinder, utilizing a hybrid Ferro-nanofluid composed of Fe_3O_4 and Al_2O_3 through the Finite Element Method (FEM) based on Galerkin weighted residual (GWR). Also, the Darcy-Brinkman-Forchheimer comprehensive approach has been used to show how fluids move through porous media. The governing parameters, including the Darcy number Rayleigh number Ha = 10, Re = 100 and various size of the cylinder have been selected to assess the impact. The computational findings of the flow and thermal fields are depicted using streamlines, isotherms, and the average heat transfer rate at the cavity's hot surface. The numerical findings show that the hybrid Ferro-nanofluid has improved HT capabilities compared to typical nanofluids, which is attributed to the synergistic effects of the nanoparticles. The circular cylinder significantly improves the strength of convection and the associated temperature gradients. A reduction in permeability suppresses fluid circulation, while larger Rayleigh numbers make stronger buoyancy-driven vortices into the cavity. The finding reveal that Fe_3O_4–Al_2O_3 HNFs and irregular porous geometries perform well for enhanced thermal management, renewable energy devices, and tiny cooling applications.

Keywords: Mixed Convection (MC), Porous Media, Hybrid nanofluids, Finite Element Method (FEM), Heat transfer.

I. INTRODUCTION

The usefulness of contemporary technological inventions, such as computer processors, material processors, electrical, micro-electrical, and nano-electrical systems, cars, and airships, can be drastically shortened by excessive heat during operation. Superheating may even cause a device to breakdown in severe surroundings. These thermal difficulties make it enormously difficult for the manufacturing industry to yield necessary machinery. As a result, it is crucial to use effective HT techniques to eliminate extra heat from these devices. While rectangular fields have been widely inspected, uneven configurations—mostly L-shaped cavities—have gained growing attention because geometric asymmetry introduces complex secondary recirculation, multi-vortex interactions, and nonlinear thermal gradients. These flow irregularities make L-shaped enclosures a reliable level for investigating natural and mixed convection behavior in progressive thermal applications [1, 2].

Significantly change the fluid flow and HT for including porous medium into the enclosure. The Darcy–Brinkman–Forchheimer model has been extensively adopted to precisely represent such combined effects in porous domains, providing a more accurate approximation of fluid momentum transport in engineering-grade porous structures [3, 4]. Numerous studies have revealed that the permeability of the porous medium strongly governs vortex formation, heat diffusion, and convective dominance, leading to substantial variation in thermal performance [5, 6].

In conjunction with geometric and porous medium complexities, research involving nanotechnology-based working fluid materials has brought about a new milestone in thermal promotion methods. HNFs consisting of two or more types of nanoparticles have been shown to be more effective than traditional nanofluids for their increased thermal conductivity, stability, and heat transportability characteristics [7]. Among many other combinations of such hybrids, it has been observed that Fe3O4 magnetic nanoparticles and Al2O3 nonmagnetic nanoparticles blended together in water present synergistic benefits together in thermal conductivity as well as magnetic controllability. The most recent developments pertaining to theoretical and practical research have reiterated that Fe3O4-Al2O3 particles present nonlinear increases in thermal conductivity along with reduced settling and magnetic field-controlled fluidity characteristics [8], [9].

The presence of an internal heated obstacle like a block further diversifies the physics inside the enclosure. The effects of internal heat sources considerably play their part in streamline development, buoyancy-driven flow creation, and HT phenomena. Many researchers have demonstrated that blocks act as ideal models to represent HGCs inside electric systems, reactors, and nuclear cooling systems [10, 11]. Nevertheless, despite numerous studies related to heat sources inside conventional enclosures, very little work can be found related to L-shaped enclosures containing heated blocks.

From a numerical perspective, GWR-FEM has been shown to be a very efficient discretized method to resolve equations for diffusion and momentum in complex domains. The ability to deal with unstructured meshes,

curved boundaries, and complex domains makes it very desirable for L-shaped domains and circular bodies, where other methods like FD methods typically encounter grid generation issues to discretize the domain [12]. Recent literature involving the application of FEM reported reliable results for MC simulation, nanofluid flow simulation, and MHD simulation inside enclosures of complex shapes, further confirming its reliability and robustness [13] and [14].

To effectively account for the coupled complexities of hybrid Ferro-nanofluid phenomena, porous media simulation, internal heating effects, and complex cavity domains, this study conducts MC HT simulation for Fe_3O_4-Al_2O_3 hybrid Ferro-nanofluid in L-shaped porous cavity involving heated block of circular form. To simulate porous fluid motion characteristics, this simulation applies DM to represent fluid motion in porous media domain. To numerically calculate solutions to transport phenomena in MC HT simulation involving complex cavity domain, it uses GWR-FEM. The findings are expected to provide deeper insight into the design of advanced HT systems, including compact cooling devices, renewable energy modules, and porous insulation components.

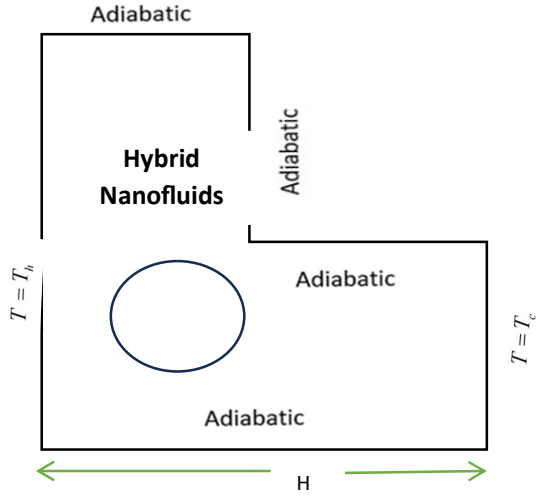

Figure 1. Schematic model and coordinate system.

II. MATHEMATICAL FORMULATION

Figure 1 shows the physical models that were used in this work. The problem has to do with two-dimensional flow into a HNF that is contained in an L-shaped porous enclosure that has a circular heated block inside it. It has copper foam as a porous medium that is filled with (Fe3O4–Al2O3) HNF and takes into account the heat generation inside (Q). The letters H stand for the length of the base wall of the enclosure. The temperature (Th) of the left wall and circular block is higher than the temperature of the right wall (Tc). The rest of the walls are kept in an adiabatic state. There is a uniform magnetic field B0 at an angle that is perpendicular to the horizontal inside the enclosure. The force of gravity (g) pulls things down. Table 1 displays the thermo physical properties of nanoparticles, base fluids, and porous materials. It is believed that there are laminar, incompressible, and unsteady flow properties. Use the Darcy-Brinkman-Forcheimer method to show how fluid flows through a porous material in this case.

TABLE 1. THERMOPHYSICAL PROPERTIES OF AL_2O_3, FE_3O_4 [8, 15] AND COPPER FOAM (40PPI) [16]

Nanoparticles				
Physical Properties	**Unit**	**Fe_3O_4**	**Al_2O_3**	**Copper Foam (40PPI)**
C_p	J/kgK	600	765	385
ρ	kg/m^3	1200	3970	9095
k	W/mK	401	40	401
σ	*s*imens/m	5.96×10^{7}	1×10^{-10}	---
$\beta\times10^5$	K^{-1}	2.67	0.85	---
ε		---	---	0.8981
K		---	---	1.28355×10^{-7}

The physical properties of this HNF remain constant, except for the density variation in the body force component of the momentum equation, which is attributed to the Boussinesq approximation. Based on these premises, the governing equations without dimensions are: (Nield and Bejan [4], & Pramanik et. al [17])

$$\frac{\partial U}{\partial X}+\frac{\partial V}{\partial Y}=0 \quad (1)$$

$$\frac{1}{\varepsilon}\frac{\partial U}{\partial \tau}+\frac{1}{\varepsilon^2}\left(U\frac{\partial U}{\partial X}+V\frac{\partial U}{\partial Y}\right)=-\frac{\partial P}{\partial X}+\frac{1}{\varepsilon}\frac{\vartheta_{hnf}}{\vartheta_{ff}}\frac{1}{Re}\left(\frac{\partial^2 U}{\partial X^2}+\frac{\partial^2 U}{\partial Y^2}\right)+\frac{\beta_{hnf}}{\beta_{ff}}\frac{Ra}{PrRe}\theta\sin\emptyset-\frac{\vartheta_{hnf}}{\vartheta_{ff}}\frac{1}{ReDa}U-\frac{F_c}{\sqrt{Da}}U\sqrt{U^2+V^2} \quad (2)$$

$$\frac{1}{\varepsilon}\frac{\partial V}{\partial \tau}+\frac{1}{\varepsilon^2}\left(U\frac{\partial V}{\partial X}+V\frac{\partial V}{\partial Y}\right)=-\frac{\partial P}{\partial X}+\frac{1}{\varepsilon}\frac{\vartheta_{hnf}}{\vartheta_{ff}}\frac{1}{Re}\left(\frac{\partial^2 V}{\partial X^2}+\frac{\partial^2 V}{\partial Y^2}\right)+\frac{\beta_{hnf}}{\beta_{ff}}\frac{Ra}{PrRe}\theta\cos\emptyset-\frac{\vartheta_{hnf}}{\vartheta_{ff}}\frac{V}{ReDa}-\frac{F_cV\sqrt{U^2+V^2}}{\sqrt{Da}}-\frac{Ha^2}{Re}\frac{\sigma_{hnf}}{\sigma_{ff}}\frac{\rho_{hnf}}{\rho_{ff}}V \quad (3)$$

$$\frac{\partial \theta}{\partial \tau}+U\frac{\partial \theta}{\partial X}+V\frac{\partial \theta}{\partial Y}=\frac{\alpha_{eff,hnf}}{\alpha_{ff}}\frac{1}{PrRe}\left(\frac{\partial^2\theta}{\partial X^2}+\frac{\partial^2\theta}{\partial Y^2}\right)+\frac{(\rho c_p)_{ff}}{\varepsilon(\rho c_p)_{ff}}Q \quad (4)$$

Here Prandtl number $Pr=\frac{\nu_{ff}}{\alpha_{ff}}$, Reynolds number $Re=\frac{U_0H}{\nu_{ff}}$, Darcy number $Da=\frac{K}{H^2}$, Rayleigh number $Ra=\frac{g\beta_{ff}(T_h-T_c)H^3}{\upsilon_{ff}\alpha_{ff}}$, Hartmann number$Ha=B_0H\sqrt{\frac{\sigma_{ff}}{\mu_{ff}}}$, and $Q=\frac{Q_0}{(\rho c_p)_{ff}(T_h-T_c)U_0}$ is heat generation.

These are the boundary conditions that are compatible with the governing equations shown earlier:

At the top, bottom, and side walls:

$U = V = 0, \frac{\partial \theta}{\partial X} = 0$

At the left wall:

$U = 1, V = 0, \theta = 1$

The left and right walls of the cavity:

$U = 0, V = 0, \theta = 0$

At the surface of the cylinder:

$U = V = 0, \frac{\partial \theta}{\partial X} = 0$

The effective thermal diffusion of the hybrid $\alpha_{eff,hnf}$ and base fluid $\alpha_{eff,ff}$ of porous medium is shown below.

$$\alpha_{eff,hnf} = \frac{\kappa_{eff,hn}}{(\rho c_p)_{hnf}} \quad \text{and} \quad \alpha_{eff,ff} = \frac{\kappa_{eff,bf}}{(\rho c_p)_{ff}} \tag{5}$$

For base fluid $\kappa_{eff,bf}$ and hybrid fluid $\kappa_{eff,hnf}$ represented respectively as:

$$\kappa_{eff,bf} = \varepsilon \kappa_{bf} + (1-\varepsilon)\kappa_s \quad \text{and} \quad \kappa_{eff,hnf} = \varepsilon \kappa_{hnf} + (1-\varepsilon)\kappa_s \tag{6}$$

The following are listed as the HNFs physical characteristics:

Following are the heat capacity [14, 18], effective dynamic viscosity [19], thermal expansion and thermal conductivity [20], the effective density [21-23] and thermal diffusivity [24] for both the nanofluid and the HNF:

$$\alpha_{hnf} = \frac{\kappa_{hnf}}{(\rho c_p)_{hnf}} \tag{7}$$

$$\rho_{hnf} = \delta_{Al_2O_3}\rho_{Al_2O_3} + \delta_{Cu}\rho_{Cu} + (1-\delta)\rho_{ff} \tag{8}$$

$$\delta = \delta_{Al_2O_3} + \delta_{Fe_3O_4} \tag{9}$$

$$\mu_{hnf} = \frac{\mu_{bf}}{\left(1-(\delta_{Al_2O_3}+\delta_{cu})\right)^{2.5}} \tag{11}$$

$$(\rho C_p)_{hnf} = \delta_{Al_2O_3}(\rho C_p)_{Al_2O_3} + \delta_{Cu}(\rho C_p)_{Cu} + (1-\delta)(\rho C_p)_{Fe_3O_4} \tag{12}$$

$$(\rho\beta)_{hnf} = \delta_{Al_2O_3}(\rho\beta)_{Al_2O_3} + \delta_{Cu}(\rho\beta)_{Cu} + (1-\delta)(\rho\beta)_{bf} \tag{13}$$

$$\frac{\kappa_{hnf}}{\kappa_{ff}} = \left(\begin{matrix}\frac{(\delta_{Al_2O_3}\kappa_{Al_2O_3}+\delta_{Cu}\kappa_{Cu})}{\delta} + 2\kappa_{Fe_3O_4} \\ +2\left(\delta_{Al_2O_3}\kappa_{Al_2O_3} + \delta_{Cu}\kappa_{Cu}\right) - 2\delta\kappa_{Fe_3O_4}\end{matrix}\right) \times \left(\begin{matrix}\frac{(\delta_{Al_2O_3}\kappa_{Al_2O_3}+\delta_{Cu}\kappa_{Cu})}{\delta} + 2\kappa_{Fe_3O_4} \\ -\left(\delta_{Al_2O_3}\kappa_{Al_2O_3} + \delta_{Cu}\kappa_{Cu}\right) + \delta\kappa_{Fe_3O_4}\end{matrix}\right)^{-1} + \frac{(\rho C_p)_{hnf}}{2}\delta\sqrt{\frac{2K_bT_{Ref}}{3\pi\mu_{hnf}d_p}} \tag{14}$$

$$\frac{\sigma_{hnf}}{\sigma_{ff}} = 1 + \left(\frac{\left(\frac{3(\delta_{Al_2O_3}\kappa_{Al_2O_3}+\delta_{Cu}\kappa_{Cu})}{\sigma_{bf}} - (\delta_{Al_2O_3}+\delta_{Cu})\right)}{\left(\frac{(\delta_{Al_2O_3}\kappa_{Al_2O_3}+\delta_{Cu}\kappa_{Cu})}{\delta\sigma_{Fe_3O_4}} + 2\right) - \left(\frac{(\delta_{Al_2O_3}\kappa_{Al_2O_3}+\delta_{Cu}\kappa_{Cu})}{\sigma_{Fe_3O_4}} - (\delta_{Al_2O_3}+\delta_{Cu})\right)}\right) \tag{15}$$

The Nu_{ave} of the enclosure's horizontally heated surface can be expressed as follows: $Nu_{ave} = -\frac{\kappa_{hnf}}{\kappa_{ff}}\int_o^H \frac{\partial\theta}{\partial Y}dX$ to the horizontally heated wall.

Where κ_{bf} is the thermal conductivity of the base fluid, T_{ref} is reference temperature, F_c Forcheimer constant, $K_B = 1.380649 \times 10^{-23}$ is the Boltzman constant and $d_p = 10$nm is the size of the particle.

III. COMPUTATIONAL PROCEDURE

The governing equations of continuity, momentum, and energy for unsteady MC of Fe_3O_4–Al_2O_3 HNF inside the L-shaped porous enclosure are solved numerically using the GWR–FEM, which is widely recommended for incompressible flow problems due to its stability and compatibility with velocity–pressure interpolation requirements [12]. The domain of computation is discretised by means of unstructured triangular elements with velocity and temperature interpolated quadratically and pressure interpolated linearly to maintain the LBB stability condition. The mesh refinement concentrates around the circular heated block, moving lids and geometrical corners as recommended for cavity-driven flows [25]. The porous medium is described by the Darcy–Brinkman–Forchheimer formulation, in which Darcy drag, viscous diffusion and nonlinear inertial resistance are directly included in the weak form [3, 19]. Magnetic effects are introduced via the quasi-static Lorentz force as an additional momentum-damping term similar to classical MHD cavity work [11]. Time-stepping is performed implicitly (Backward Euler), and convection as well as Forchheimer nonlinearities are linearized with Picard or Newton iterations for the purpose of a robust solver design. The thermo-physical properties of the HNF – density, viscosity, heat capacity, thermal conductivity, expansion coefficient and electrical conductivity – are computed iteratively at each time step using mixture-based correlations and hybrid enhancement models based on recent formulations of HNF [7, 17]. Convergence is achieved when the L2-norm of successive iterations satisfies a tolerance of 10^{-6} for velocity, pressure, and temperature fields. The numerical solver is verified through grid- and time-independence studies and validated by reproducing classical benchmark solutions for MC in cavities and porous media as reported in Aydin [1], Abu-Nada et al. [6], and natural-convection benchmarks. After convergence, streamlines, isotherms, and Nuave are computed to analyze the thermal and flow performance of the HNF system.

IV. VALIDATION

The numerical model was verified and validated through multiple systematic steps. Code verification was first performed using the method of manufactured solutions on a simplified set of governing equations (excluding Forchheimer and MHD effects) to ensure correct implementation of the solver. Further verification involved

comparison against classical benchmark cases, such as the lid-driven cavity flow at Re = 100 for a pure fluid, confirming the accuracy of the velocity and pressure fields. To extend validation to nanofluid simulations, single nanofluid results from literature—such as Al_2O_3/water natural convection in a cavity [6]—and hybrid Cu–Al_2O_3/water cases reported by Pramanik et al. [26] were successfully reproduced.

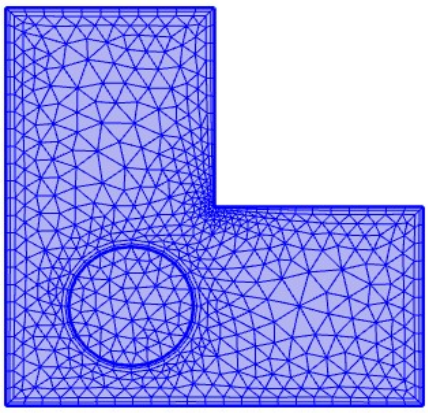

Figure 2. Standard Finite Element discretizing a L-shape Cavity

V. TEST FOR GRID REFINEMENT

The mesh quality is also shown in Figure 2 by the grid design of the present physical domain, which has triangular finite elements. For this research, triangular quadratic finite elements with six nodes are applied to mesh the complicated geometry for improved precision. This article is two-dimensional L-shaped porous chambers incorporating a circular cylinder. Inside the structure, grid size sensitivity assessment was carried to assess the adequacy of the meshing system in Figure 2 and confirm the grid independence test of the outputs. The solution is guaranteed to be grid-independent by collecting numerical results for many grid sizes. In Table 2, you can see the Nuave along the left heated wall, which was determined with different levels of mesh fineness. For each iteration of the improved mesh, the number of components is quadrupled compared to the one before it. Since the table's last column clearly shows that the mesh refinement from the third to fourth level reduces the percentage error of solutions to as low as 2.8897%, thus here utilized the 3rd iteration level (a random mesh of 1790 elements) to generate numerical outcomes across the text.

TABLE 2. NU_{AVE} DISPLAYED ALONG THE BOTTOM WALL FOR DIFFERENT MESH SIZES.

Refinements	No. of elements	Nu_{ave}	% Error
1st	113	0.5051	2.9497
2nd	624	0.3572	3.0657
3rd	1790	0.4671	2.9339
4th	6585	0.5078	2.8897

VI. Results and Discussion

The effects of HT on various Darcy (Da) and Rayleigh numbers (Ra) are analyzed to study the characteristics of the flow and temperature fields in an L-shaped cavity containing a circular cylinder. The current numerical study examines the parametric domains of the dimensionless groups $10^{-5} \leq Da \leq 10^{-1}$, $10^{5} \leq Ra \leq 10^{10}$, Re = 100, and Ha = 10.

6.1 Effect of Darcy Numbers (Da)

Figure 3 shows the streamlines in the L-shaped cavity, which change with different Darcy numbers and cylinder sizes. When the Darcy number is high (10^{-1}), the porous medium allows the fluid to move easily, so the flow is strong and forms big vortices around the cylinder. At a medium Darcy number (10^{-3}), the flow becomes weaker and the vortices are smaller. At a very low Darcy number (10^{-5}), the porous resistance is high, so the flow moves slowly and the streamlines become smooth with almost no strong circulation. Cylinder size also affects the flow: small cylinders disturb the flow slightly, medium-sized cylinders create stronger vortices, and large cylinders block the flow and create bigger stagnant zones.

Figure 4 shows how heat spreads inside the L-shaped cavity for different Darcy numbers and cylinder sizes. When the Darcy number is high (10^{-1}), the fluid moves more freely, so the hot and cold temperature lines bend strongly and spread widely around the cylinder. At a medium Darcy number (10^{-3}), the temperature lines become smoother, and heat spreads less because the flow is weaker. At a very low Da (10^{-5}), the porous medium blocks the flow, so the isotherms stay almost straight and heat spreads mainly by conduction. Cylinder size also affects the temperature field: small cylinders have little influence, medium cylinders disturb the isotherms more, and large cylinders block the heat path, causing stronger temperature gradients around the obstacle.

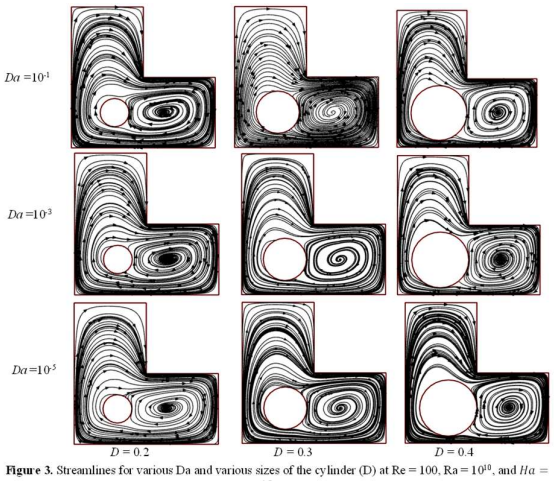

Figure 3. Streamlines for various Da and various sizes of the cylinder (D) at Re = 100, Ra = 1010, and Ha=10.

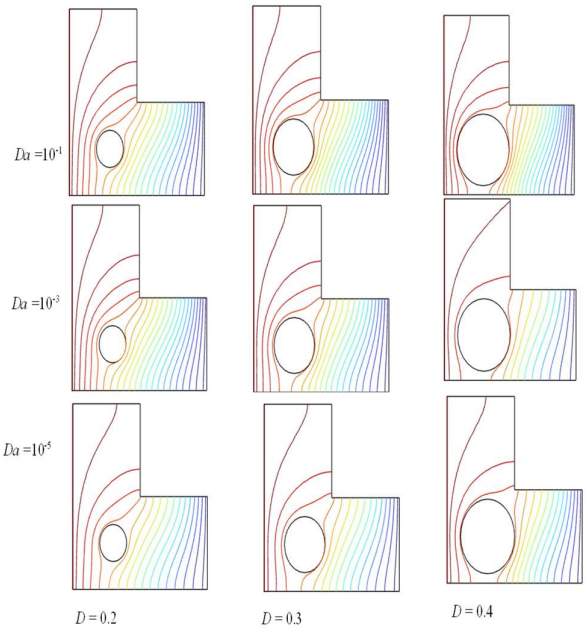

Figure 4. Isotherms various Da and various sizes of the cylinder (D) at Re=100, Ra = 10^{10}, and

Figure 4. Isotherms various Da and various sizes of the cylinder (D) at Re=100, Ra = 1010, and

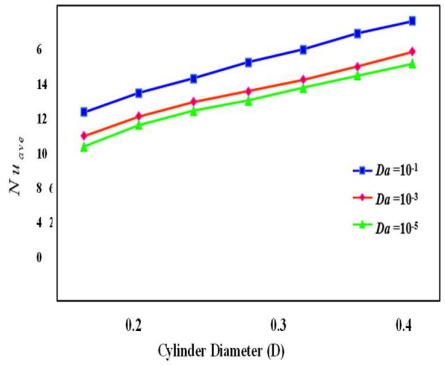

Figure 5. The distinction of Nu_{ave} for various Da and D with Re =100, and $Ra = 10^{10}$.

Figure 5. The distinction of Nuave for various Da and D with Re =100, and

Figure 5 shows the variation of the Nuave along the heated surface for different Darcy numbers (Da) and cylinder diameters (D) at fixed parameters of Re = 100 and Ra = 1010. It is revealed that the porous permeability as well as the cylinder size play a significant role in the HT rate inside the cavity. As Darcy number increases, the porous material forms less resistance to the flow such that more convection can take place. As a result, more fluid mixing is achieved and subsequently an enhanced Nuave. This tendency is also observed with the cylinder diameter as well since larger ones disturb the flow field more effectively, which forms stronger circulation zones leading to improvements in convection HT. In all the cases, the maximum Nuave corresponds to the largest obstacle (D = 0.4) at the highest Darcy number, which is consistent with enhanced flow permeability and larger obstacle size favoring a stronger convective HT for this system.

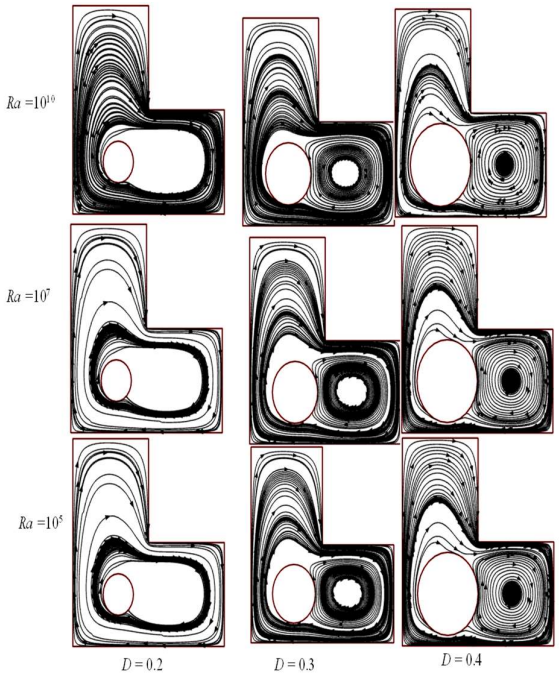

Figure 6. Streamlines various Ra and various sizes of the cylinder (D) at Re=100, Da = 10^{-2}, and

Figure 6. Streamlines various Ra and various sizes of the cylinder (D) at Re=100, Da = 10-2, and Ha=10.

6.2 Effect of Rayleigh Numbers (Ra)

The streamlines in the L-shaped cavity change clearly with different Rayleigh numbers and cylinder sizes are investigated in Figure 6. At a low Rayleigh number (Ra= 〖10〗^5), the influence of the moving lid is predominant and only one primary giant vortex develops in the cavity. With the increase in Ra to Rayleigh number of 〖10〗^7, the buoyancy effect becomes more prominent and flow in vicinity of the heated left wall becomes stronger and there will be more circulation intensity around cylinder. When Ra= 〖10〗^10 buoyancy force is the most effective and very strong and compact vortices are observed especially near the heated wall and all-around cylinder. The size of the cylinder also has an influence on the flow structure: a smaller cylinder (D = 0.2) allows for a more open flow, which results in smoother flow. As D increases the wake becomes less regular and small secondary vortices are generated in its wake (D = 0.3). For the largest cylinder (D = 0.4) the fluid passage is very tight and streamlines are much denser resulting in intense recirculation zones developed within the domain. In general, more powerful flows are generated with larger Rayleigh numbers; the larger cylinders obstruct flow more and induce stronger local vortices within the L-shaped enclosure.

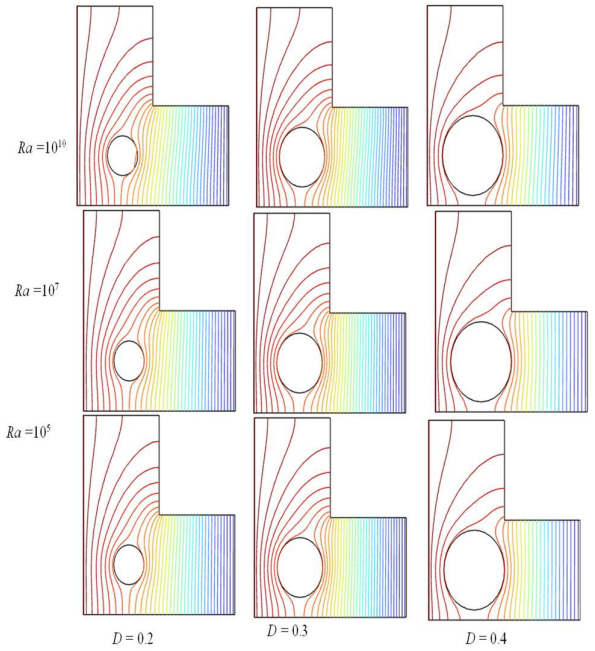

Figure 7. Isotherms for various Ra at Da=10^-2, δ = 0.05, and Ha = 10.

Figure 7. Isotherms for various Ra at Da=10-2, and Ha=10.

The isotherm graphics shown in Figure 7indicate certain aspect of the influence due to Ra and cylinder size on temperature field inside L-shaped cavity. The similarity of the solutions for both Ra is manifest, Rh face — produces a trend towards linearity such that high Rayleigh number behaving as expected since when low it-HT is almost completely conduction dominated giving smooth and many concentrations move rapidly perpendicularly to the left hot wall (in- closely spaced contours flowing across the domain. When the Rayleigh number is 〖10〗^7, convection becomes stronger and isotherms bend more to the right of cavity. This buckling indicates that there is an upward motion of warm fluid near the hot wall and cold fluid moving toward the cylinder. Strong isotherms' curvature and compression of their shape around the heated wall and at large values close to cylinder indicate faster heat transfer properties under highest Rayleigh number (Ra= 〖10〗^10) due to strong convection. The temperature field is also sensitive to the cylinder size: a small (D = 0.2) one produces only small deflection of isotherms, but increase in D (in this case to 0.3) makes them wrap more steeply around the object. In the largest cylinder (D = 0.4) the isotherms are narrowly spaced along the cylinder and cavity walls, indicating strong temperature gradients and larger HT rates. Overall, higher Rayleigh numbers strengthen convective HT, while larger cylinders increase temperature distortion and create stronger thermal gradients inside the L-shaped enclosure.

Figure 8 shows that, at fixed Da = 10-2, and Re = 100, as Ra increases from 105 to 1010, the Nuave rises for all cylinders. The largest HT occurs at Ra = 1010 with D = 0.4, while the smallest occurs at Ra = 105 with D = 0.2.

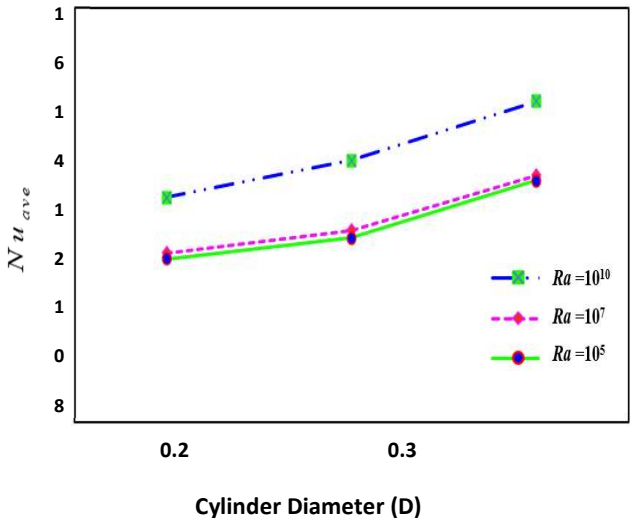

Figure 8. The distinction of Nuave for different Ra and D with Re = 100, and Da=10^(-2).

VII. CONCLUSIONS

The numerical study of MC flow and HT in an L-shaped porous cavity with a circular cylinder shows that the Darcy number, Rayleigh number, and cylinder size strongly influence the overall behavior of the system. For high Darcy numbers (Da = 10^{-1}), the porous medium allows the fluid to move easily, producing strong circulations, large vortices, and noticeable bending of isotherms, which together improve convective HT. When the Darcy number decreases to 10^{-3}, the flow becomes weaker and HT reduces because convection loses strength. At extremely low Darcy numbers (Da = 10^{-5}), the porous resistance becomes dominant, resulting to struggling fluid motion and practically conduction-controlled HT with smooth streamlines and relatively straight isotherms.

The Rayleigh number (Ra) has a large effect on HT phenomena. The larger the Ra number, the greater will be the buoyancy effects, fluid motion, and phenomena of convection. The lower Ra number reduces fluid motion; HT becomes conductive in nature if the values of the Darcy numbers are small.

The scale of the cylinder affects the nature of flow. Small amounts of shaking occur in small cylinders. Moderate cylinders help to improve vortex creation and temperature differences because of increased fluid interruption. Relatively large cylinders cause restrictions to fluid flow past the barrier to form areas of fluid stagnation and large temperature differences.

In conclusion, the effects of Da number, Ra number, and size of the cylinder characterize the transport of heat and fluid inside the L-shaped porous cavity. Large Da and Ra numbers cause strong convection currents; conversely, small values of both numbers result in situations ideal for heat conduction. These results have great significance in thermal systems configuration by considering variations in the dimensions of the cylinder to ensure optimal performance of HT.

VIII. ACKNOWLEDGEMENT

The authors are thankful to Dhaka International University, Dhaka, Bangladesh, for all kinds of research support.

REFERENCES

[1]. O. Aydin, "Adding and opposing mechanisms of mixed convection in a shear- and buoyancy-driven cavity." International Communications in Heat and Mass Transfer, 26(7), 1999, pp. 1019–1028.

[2]. Q. Deng, C. Lei, J. C. Patterson, "Natural convection in L-shaped enclosures: A review." International Journal of Heat and Mass Transfer, 135, 2019, pp. 1–12.

[3]. K. Vafai, C. L. Tien, "Boundary and inertia effects on flow and heat transfer in porous media." International Journal of Heat and Mass Transfer, 24(2), 1981, pp. 195–203.

[4]. D. A. Nield, A. Bejan, Convection in Porous Media. 5th Edition, Springer, 2017.

[5]. K. Khanafer, K. Vafai, M. Lightstone, "Buoyancy-driven heat transfer enhancement in a two-dimensional enclosure utilizing nanofluids." International Journal of Heat and Mass Transfer, 46(19), 2003, pp. 3639–3653.

[6]. E. Abu-Nada, Z. Masoud, H. F. Oztop, A. Campo, "Effect of nanofluid variable properties on natural convection in enclosures." International Journal of Thermal Sciences, 49(3), 2010, pp. 479–491.

[7]. J. Sarkar, P. Ghosh, A. Adil, "A review on hybrid nanofluids: Recent research, development and applications." Renewable and Sustainable Energy Reviews, 43, 2015, pp. 164–177.

[8]. Y. Cao, "Combination effect of Fe_3O_4 and Al_2O_3 nanoparticles on water-based hybrid nanofluids." 2023.

[9]. Liu, H., & Zheng, X. "Rheological synergistic thermal conductivity of Fe_3O_4–Al_2O_3 hybrid nanofluids under shear flow." 2023.

[10]. M. M. Billah, M. M. Rahman, M. H. Kabir, U. M. Sharif, "Heat transfer and flow characteristics for MHD mixed convection in a lid-driven cavity with heat generating obstacle." International Journal of Energy & Technology, 3, 2011.

[11]. T. Javed, Z. Mehmood, I. Pop, "MHD mixed convection flow in a lid-driven trapezoidal cavity under uniformly/non-uniformly heated bottom wall." International Journal of Numerical Heat & Fluid Flow, 27(6), 2017, pp. 1231–1248.

[12]. C. Taylor, P. Hood, "A numerical solution of the Navier–Stokes equations using the finite element technique." Computers & Fluids, 1(1), 1973, pp. 73–100.

[13]. A. Siddiqua, S. Parvin, "Heatline analysis for MHD mixed convection flow in a cavity with heat generating block." AIP Conference Proceedings, 1754, 2016.

[14]. H. A. Nabwey, A. M. Rashad, P. B. A. Reddy, "Radiative effect on unsteady MHD natural convection in an inclined porous cavity using hybrid nanofluid." Alexandria Engineering Journal, 65, 2023, pp. 921–937.

[15]. H. D. Touki, M. N. Hossain, , A. I. Ferdous, Y. Hoque,, Ahmed, M., Saha, S., "Thermal management of micropolar ferrofluid forced convective flow in a T-shaped vented chamber via a proportional-integral-derivative controller", South African Journal of Chemical Engineering, Volume 55, 2026, pp. 222-234, ISSN 1026-9185.

[16]. I. Y., Hossain, M. A. Jasim, "Thermal Performance Enhancement of Phase Change Materials (PCMs) by Using Metal Foams", Al-Nahrain Journal of Engineering Science (NJES), 20(1), 2017), pp. 235-249.

[17]. M. A. R. Pramanik, M. M. Billah, A. R. Khan, B.I. Chowdhury, ATM. M. Rahman, M. Mandol, (2023). MHD hybrid nanofluid in porous cavity using FEM. Proceedings of ICME 2023.

[18]. C.S. Balla, A. Ramesh, N. Kishan, A.M. Rashad, Z.M.A. Abdelrahman, "Bioconvection in oxytactic microorganism saturated porous square enclosure with thermal radiation impact", Journal of Thermal Analysis and Calorimetry, 140 (50), 2020) pp. 2387-2395.

[19]. H.C. Brinkman, "The velocity of concentrated suspensions and solutions", (J. Chem. Phys. 20(4), 1952) pp. 571.

[20]. J.A. Maxwell, "Treatise on Electricity and Magnetism", (IOP Publishing, 1904).

[21]. E. Abu-Nada, Z. Masoud, H.F. Oztop, A. Campo, "Effect of nanofluid variables properties on natural convection in enclosures", Int. J. Therm. Sci. 49 (3), 2010) pp. 479–491.

[22]. K. Khanafer, K. Vafai, M. Lightstone, "Buoyancy-driven heat transfer enhancement in a two-dimensional enclosure utilizing nanofluids", (Int. J. Heat Mass Transf. 46 (19), 2003) pp. 3639–3653.

[23]. S. Jana, A. Salehi-Khojin, W. H. Zhong, "Enhancement of fluid thermal conductivity by the addition of single and hybrid activities", Thermochimica Acta, 462 (1-2), 2007) pp. 45–55.

[24]. C.J. Ho, J.B. Huang, P.S. Tsai, Y.M. Yang, "Preparation and properties of hybrid water-based suspension of Al2O3 nanoparticles and MEPCM particles as functional forced convection fluid", International Communications in Heat and Mass Transfer 37(5), 2010), pp. 490–494.

[25]. O. Aydin, (1999). Mixed convection in a shear- and buoyancy-driven cavity. Int. Commun. Heat Mass Transfer, 26, 1019–1028.

[26]. M. A. R. Pramanik, M. M. Billah, A. R. Khan, Heat transfer augmentation in a double lid-driven trapezoidal porous cavity with heated block using hybrid nanofluid, International Journal of Thermofluids, 24 (2024) 100924.